Progress In Electromagnetics Research B, Vol. 68, 123–140, 2016

Extended Transmission-Line Modelling of Inset-Fed Reconfigurable Rectangular Microstrip Antennas

Budhaditya Majumdar* **and Karu Esselle**

Abstract—An extended transmission-line model is presented for an inset-fed rectangular microstrip patch antenna. The transmission-line model agrees to the $\cos^4$ impedance variation for inset-fed microstrip antennas with an addition of a corrective extended feed length upto the inner radiating edge. Verification of the model's complex reflection coefficient is concluded with good agreements with measured results. Further extension of the transmission-line model with for or more thin shorting post connected to multiple varactor diodes have been conducted. Fourty two test cases across five independent antenna designs have been worked upon. Results obtained using the transmission-line model are compared with those obtained with a 3D full-wave solver and measurements. In 69% of the test cases, the transmission-line models have less than 3% deviation to the measured or simulated results. 41% of them have less than 1% deviation. For the first two antennas, both simulated and measured results were compared with the transmission-line model. For the rest of three, results from the transmission-line model were compared to the simulated ones.

1. INTRODUCTION

Rectangular microstrip antennas have been around for over half a century and numerous experimental and theoritical studies have been conducted. The transmission-line model of the rectangular microstrip patch antenna [1–5] was discussed in many occasions, and the variation of input impedance was primarily investigated with respect to the location of the feed probe [3–5]. Analysis of the inset-feed is not very proclaimed in the literature. Some of the empirical works done in the recent past are focused on the $\cos^4$ reduction of input impedance [6, 8] instead of the traditional $\cos^2$ reduction mentioned in the early literatures [3–5]. Another formulation for designs with the inset very close to the centre is based on the shifted $\cos^2$ was recently presented [6, 7]. This work implements the $\cos^4$ reduction formula with a new corrective inset-feed length extension.

Shorted microstrip patch antennas have been analysed in various forms. The earliest form of patch reduction was done by shorting the microstrip patch antenna size along the H-plane [9]. Further improvements about size reduction can be achieved by the help of multiple shorting posts instead of using one long and continuous metal strip across the H-plane [10–12]. Transmission-line modelling of rectangular microstrip patch antenna with shorting posts along the line of magnetic symmetry to demonstrate the change of antenna resonance frequency have also been discussed [13, 14]. The aforesaid model only considered posts placed in the centre of the width of the patch but at any position along the length (E-plane). Similar tuning with circular patch antennas are also possible [15, 16]. Accurate results can also be obtained for shorted microstrip antennas using cavity model and this was presented for circular patch antennas [17, 18]. Rectangular microstrip antennas can be designed to have their non-radiating edges shorted to ground to significantly reduce cross polarized radiation and was recently analyzed using the cavity model [19]. Compact designs and larger impedance can also be achieved

Received 15 April 2016, Accepted 6 June 2016, Scheduled 14 June 2016
* Corresponding author: Budhaditya Majumdar (budhaditya.majumdar@ieee.org).
The authors are with the Department of Engineering, Macquarie University, Sydney, NSW 2109, Australia.

using a secondary coupled patch with shorting posts implemented in both the primary and secondary patches [20]. Models of rectangular microstrip antennas with shorting posts placed at various positions of the outer radiating edge to tune the antenna was recently communicated [21, 22]. A design with shorted circular patch over a ring resonator for multiband operation was also recently communicated [23]. Transmission line modelling for rectangular patch antenna with superstrates are also possible and was recently communicated [24].

Use of variable capacitors or varactor diodes for polarization agility was mentioned as early as 1981 [13, 25] and was extended for arrays later [26–28]. The next improvement happened with the use of a BAR28 Schottky barrier diode operating in reverse bias to reconfigure the resonance frequency [29]. Further modelling and investigations were also discussed with respect to probe fed microstrip patch antennas and arrays loaded with varactor diodes (Schottky barrier diodes) [30–32]. A detailed model and explanation of a varactor loaded patch antenna can again be found in [33]. A cavity model of varactor loaded circular microstrip antenna can be found in [34]. Improvement of scan performance of microstrip patch array antennas are also possible by using shorting posts and diodes [35] and possibility of using diodes to replace the shorting posts were discussed in the past. Multiple diodes were also mentioned in the past for polarization agility [27, 28] and also for dual frequency operations [31]. Modern polarization agile microstrip antennas use only a SPDT switch with a hybrid coupler to limit design complications and efficient operation [36]. polarization agility is In most of the previously mentioned papers, the diode is modelled inside a hole similar to a via or shorting post, and may have been difficult to solder. With present day packaging of RF diodes (e.g., SC-79 package), they would be impossible to solder inside a hole to replace a shorting post, as mentioned in the literature. Resistor loading was investigated as a replacement of shorting posts and varactor diodes and it was found that resistor loading benefits the return-loss bandwidth up to an extent [37, 38].

While most of the publications have focused on the benefits of using a diode for various kinds of reconfigurability, this paper focusses on the accuracy of inset-feed transmission-line modelling of the rectangular microstrip antenna and its extension with one or more diodes. Multiple diodes were used to emulate a diode with higher junction capacitance to test the transmission-line model rigorously. Most previous publications (to the best of the authors' knowledge) have discussed the probe fed models only with return-loss diagrams of calculated and measured results [13, 32, 33] but in this paper the authors implemented and verified an empirically model of inset-feed, which is rarely discussed, with complex impedance results plotted on a Smith chart. The transmission-line model of a rectangular microstrip patch antenna [1–5] is modified to archetype the effect of the one or more varactor diodes and vias. Fourty two test cases are used to obtain the highly accurate and less accurate results across five different reconfigurable rectangular microstrip antennas.

2. MICROSTRIP PATCH TRANSMISSION-LINE MODEL AND INSET-FEED

The transmission-line model for a rectangular microstrip antenna has been extensively discussed in the literature [1–5]. Two slots, each having a complex admittance, are placed at a distance of about $\lambda_{eff}/2$ [5]. For a standard rectangular patch antenna, each of the complex slot admittance is denoted by $G + jB$ where G is the slot conductance and B is the slot susceptance, respectively. The formulas for the slot conductance and susceptance are given in [5].

The input admittance of the conventional rectangular microstrip patch antenna can be given expressed as [2]:

$$Y_{inp}^{0} = G + jB + Y_p \frac{G + j\left(B + Y_p \tan kL_P\right)}{Y_p - B\tan kL_P + jG\tan kL_P} \tag{1}$$

where k is the effective wave number. L_P is the length of the patch, and Y_p is its respective characteristic admittance.

Inset feeding is a popular feeding technique which is often used to lower the edge impedance and helps in keeping the width of the microstrip line feed realistic and manufacturable. Conventionally the inset probe feed is modelled with a admittance incremental factor defined by $\sec^2(\frac{\pi}{L_P}L_{in})$ [3–5] and some publications have proposed the same for microstrip line inset-feeds as well. This theory has been contradicted in the recent past [6–8] and a new admittance factor of $\sec^4(\frac{\pi}{L_P}L_{in})$ has been proven to

be more accurate for microstrip line inset-feeds where the feed end is closer to the inner edge of the microstrip patch. In the empirical models published lately [6–8], the aspect ratio of the patch (W_P/L_P) is considered to be 1.5 and inset-gap to inset-feed width ratio (W_{in}/W_T) is 3. In the base designs mentioned in this paper the aspect ratio is 1.21 & 1.36, and the inset-gap to inset-feed width ratio is 3.73 & 4. The overall antenna admittance used for multiple antenna designs are derived in Section 4 along with the extended transmission-line model.

3. ANTENNA CONFIGURATIONS

Five separate antenna designs are discussed below in different subsections. All the five antennas are based on two major base designs of rectangular microstrip patch antennas. Two different substrates and different resonance frequencies are used for the design of the base antennas. The base antennas are modelled and manufactured first and compared with calculated results to verify the accuracy of the inset-fed microstrip patch transmission-line model. Five extended reconfigurable antennas are then designed and verified with transmission-line results. All of them follow the same design layout shown in Fig. 1(a) with the exception of last one, which is given in Fig. 1(b). Actual dimensions, diode configurations and the substrate used for the design of antennas are given below.

3.1. Base Antenna Designs

A low-permittivity substrate, Rogers 5880 ($\epsilon_r = 2.2$, $\tan\delta = 0.0009$) with a thickness of 0.787 mm was used to design and manufacture the first fundamental microstrip patch antenna. This design will be known as 'Base Design I' for the rest of the paper. The length and width of the substrate are $L_{S1} = 120$ and $W_{S1} = 100$ mm, respectively. The length and width of the patch are $L_{P1} = 58$ mm and $W_{P1} = 70$ mm, respectively. Matching has been achieved with a quarter wave transformer, which is directly connected to the 50 Ω feed-line. The length and width of the transformer are are $L_{T1} = 31$ mm and $W_{T1} = 1.1$ mm, respectively. The length and width of the feed-line are $L_{50\Omega 1} = 17.5$ mm and $W_{50\Omega 1} = 2.25$ mm, respectively. The cut-out of the inset has the dimensions are $L_{In1} = 10$ mm and $W_{In1} = 4.1$ mm, respectively. The aspect ratio of the patch (W_{P1}/L_{P1}) is 1.21 and the inset-feed width ratio (W_{in1}/W_{T1}) is 3.73.

A Taconic TRF-43 substrate ($\epsilon_r = 4.3$, $\tan\delta = 0.0035$), having a thickness of 1.2 mm was for the second fundamental microstrip patch antenna, 'Base Design II'. Similar to 'Base Design I', the design is shown in Fig. 1(a) but with different values. The length and width of the substrate are $L_{S2} = 70$ mm and $W_{S2} = 65$ mm, respectively. The length and width of the patch are $L_{P2} = 31$ mm and $W_{P2} = 42$ mm, respectively. The length and width of the transformer are $L_{T2} = 15.5$ mm and $W_{T2} = 1$ mm. The length and width of the feed-line are $L_{50\Omega 2} = 20$ mm and $W_{50\Omega 2} = 2.2$ mm, respectively. The cut-out of the inset has the dimensions $L_{In2} = 8$ mm and $W_{In2} = 4$ mm, respectively. The aspect ratio of the patch (W_{P2}/L_{P2}) is 1.36 and the inset-feed width ratio (W_{in2}/W_{T2}) is 4.

3.2. Varactor Loaded Antenna Designs

Reconfigurability is implemented in the 'Base Design I' with the help of an actively operated via located close to one of the outer vertex opposite to the feed in the patch element. Figs. 1(c), (i) show the photograph of 'Antenna I'. The via is connected between the patch and a small island in the ground plane (Figs. 1(c), (ii)). An annular gap separates the island from the greater ground plane. One or few varactor diodes are connected across this gap and they act as a load on the radiating slot of the patch antenna. In 'Antenna I' only one varactor diode is used. The outer and inner diameter of gap surrounding the island are are $D_I = 4$ mm and $D_{I'} = 3$ mm. The via is formed by a 18AWG wire with a diameter (D_{Via}) of 1 mm. The diode(s) make an impedance bridge across the terminals of the SMA port and only a DC offset with correct polarity is required across the SMA port to control the state of the varactor diode(s), which can be either forward or reverse biased. This design methodology completely eliminates the requirement of any printed bias lines or dangling bias wires that can affect the resonance frequency and gain. Instead, only a bias-tee is required for tuning.

'Base Design II' is modified with an actively operated via, similar to 'Antenna I' to form 'Antenna II'. It also has only one varactor diode bridging the annular gap between the island and the greater

ground plane. Figs. 1(c), (iii) show the photograph of 'Antenna II'. 'Antenna I' with two varactor diodes bridging the annular gap forms 'Antenna III'. This is done to effectively double the junction capacitance at the same point of operation. Every thing else in the design remains the same. 'Antenna II' with two varactor diodes bridging the annular gap forms 'Antenna IV'. Similar to the previous design, nothing

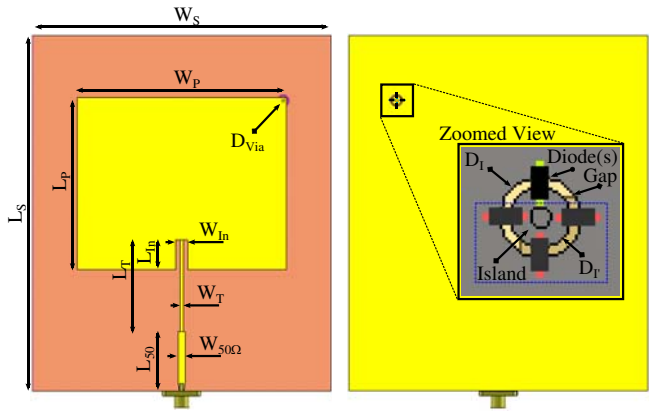

(a) Layout used for Antenna I - IV

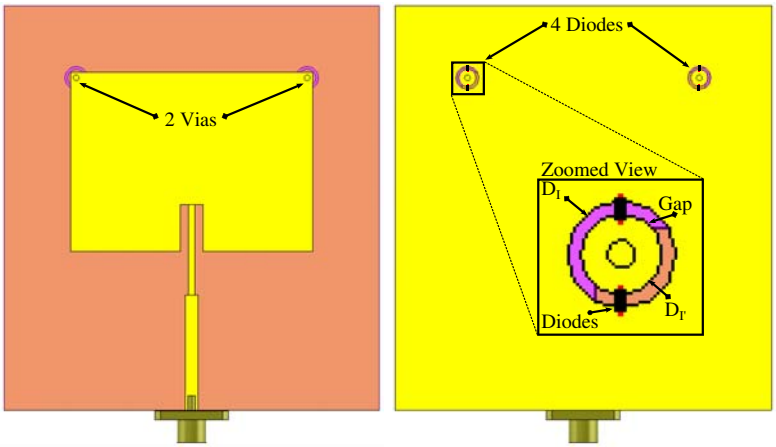

(b) Layout used for Antenna V

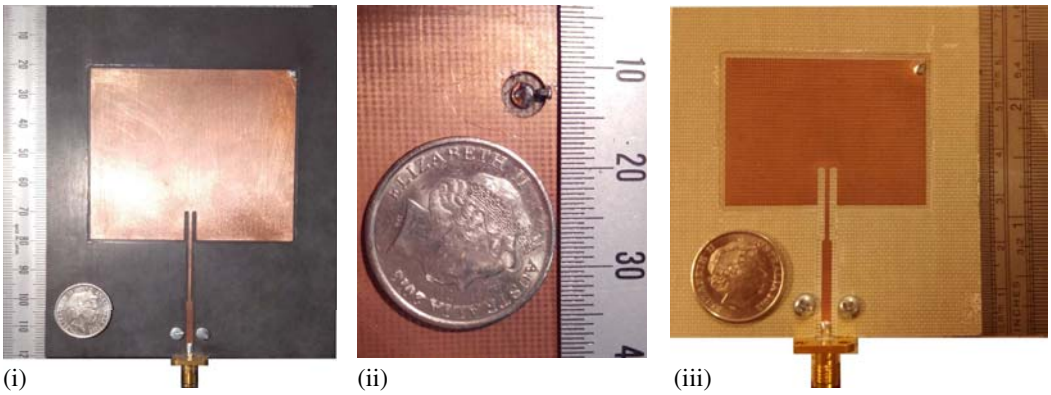

(i) (ii) (iii)

(c)

Figure 1. Layout (top and bottom view) of the investigated antennas (a) for Antenna I to IV, and (b) for Antenna V; along with the fabricated patch antennas showing (c)(i) the top view of 'Antenna I' with the short at the upper right vertex, (c)(ii) zoomed in view of a varactor diode soldered to the island in the ground plane, in comparison to an Australian five-cent coin, and (c) (iii) the top view of 'Antenna II' with the short at the upper right vertex of the patch.

else is modified. 'Antenna V' has same design values from 'Antenna II' but has two vias connected to two local islands and the two vias are located at the two outer vertices of the patch. Fig. 1(b) shows the top and bottom view of 'Antenna V'. Similar to 'Antenna IV', each island has two varactor diodes bridging the annular gap, with a total of four varactor diodes used for this antenna. Due to the magnetic symmetry of the rectangular patch [22], the effective value of the via and diodes would double up. This is further explained in the next section. Tuning is achieve with the same bias-voltages and polarities as used for the previous designs.

4. EXTENDED TRANSMISSION-LINE MODEL

When a thin via ($D_{Via} \ll W_P$) is soldered at the outer vertex of the rectangular patch, it can be approximated that the admittances of both the slots have the same values as before, with the susceptance of the via, $-j/\omega L_{sh}$, added in parallel to the complex admittance of the outer slot [21]. With an island created and a varactor diode soldered to bridge the island and the greater ground plane as shown in Fig. 1, the transmission-line model can be extended as shown in Fig. 2(a). Depending on diode polarity, the transmission-line model changes to represent the state of the varactor diode. A forward-bias diode conductance G_{VarD} or a reverse-bias junction susceptance ωC_{VarD} along with the package lead susceptance $-j/\omega L_{VarD}$ is added in series with the via susceptance. Then the patch input admittance for the extended transmission-line model is given by:

$$Y_{inp} = G + jB + Y_p \frac{G + j\left(B - \Psi + Y_p \tan kL_P\right)}{Y_p - (B - \Psi)\tan kL_P + jG \tan kL_P} \tag{2a}$$

where

$$\Psi = \frac{G_{VarD}}{\omega G_{VarD}\left(L_{sh} + L_{VarD}\right) - j} \tag{2b}$$

in the forward-biased mode, and

$$\Psi = -\frac{\omega C_{VarD}}{1 - \omega^2 C_{VarD}\left(L_{sh} + L_{VarD}\right)} \tag{2c}$$

in the reversed biased mode, k is the effective wave number and Y_p is the characteristic admittance of the patch. Notice that in the forward-biased mode, junction susceptance ωC_{VarD} is ignored. Likewise diode conductance G_{VarD} is ignored for reverse-biased mode.

4.1. Antenna Admittance

The overall antenna admittance depends on the length of the inset, quarter wave transformer and the $50\,\Omega$ feed-line, respectively. Admittance for an inset-fed patch is given by [6, 8]:

$$Y_{inp'} = Y_{inp} sec^4\left(\frac{\pi}{L_P} L_{In}\right) \tag{3}$$

where L_{in} is the inset-feed length, and Y_{inp} is the edge admittance of the patch as given in Eq. (1) or Eq. (2) depending on the absence or presence of the thin shorting post and additional diodes. Another admittance transformation takes place with the quarter-wave transformer and the admittance of the patch at the input of the quarter-wave transformer is given by:

$$Y_{inp''} = Y_T \frac{Y_{inp'} + jY_T \tan k\left(L_T + 1.25L_{In}\right)}{Y_T + jY_{inp'} \tan k\left(L_T + 1.25L_{In}\right)} \tag{4}$$

where L_T is the length of the quarter-wave transformer, and Y_T is the characteristic admittance of the transformer.

In the process of this research it was empirically found out after comparison with measurement results that the complex impedance obtained from the extended transmission-line model match up with the measurements and simulations when a corrective feed length to the inner radiating edge is considered. The corrective feed length from the feed point to the inner radiating edge is equal to the length of the inset (L_{In}) with a linear co-efficient of 1.25, thus making the total feed length equal to

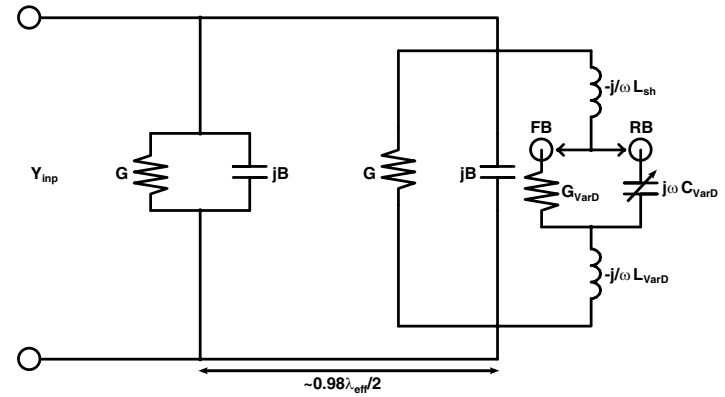

(a) Transmission-line model diagram for Antenna I and II

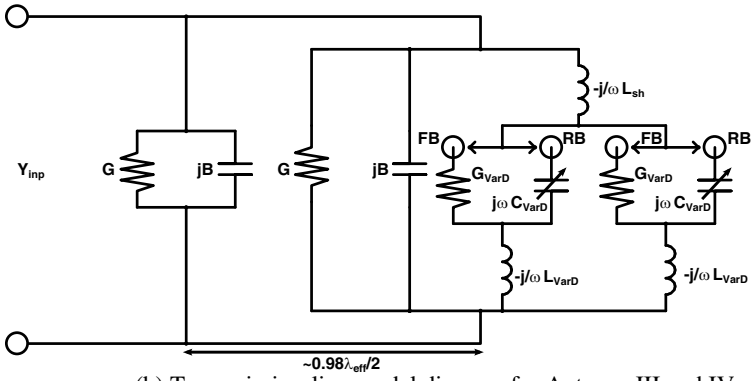

(b) Transmission-line model diagram for Antenna III and IV

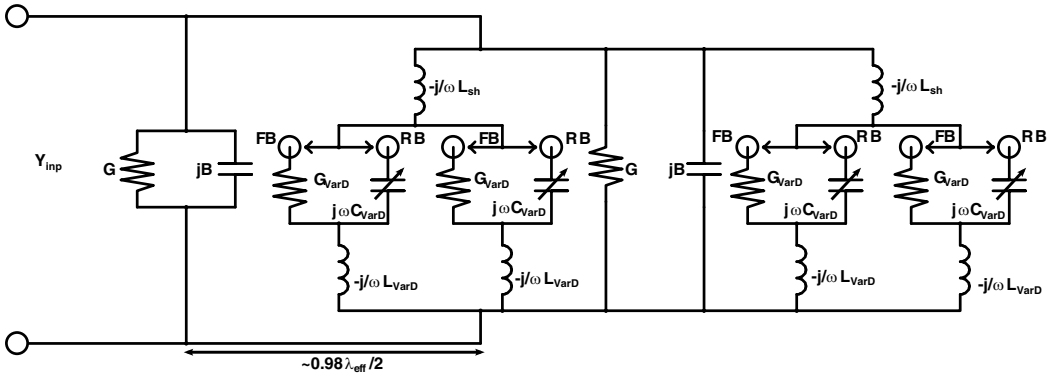

(c) Transmission-line model diagram for Antenna V

Figure 2. Extended transmission-line model diagrams of the five antennas investigated in this paper.

the length of the quarter wave transformer (L_T) added to the corrective feed length ($1.25L_{In}$) making it equal to $L_T + 1.25L_{In}$.

The overall admittance at the SMA port is given by:

$$Y_{inp50\Omega} = Y_{50\Omega}\frac{Y_{inp''} + jY_{50\Omega}\tan kL_{50\Omega}}{Y_{50\Omega} + jY_{inp''}\tan kL_{50\Omega}} \tag{5}$$

where $Y_{50\Omega}$ is approximately $0.02S$, and $L_{50\Omega}$ is the length of the feed-line (till the measurement plane of the SMA Port) as shown in Fig. 1.

4.2. Admittance with Two Diodes

More than one varactor diodes can be connected across the annular gap to connect one via to the ground plane. The extended transmission-line model with two varactor diodes connected to one via is shown

in Fig. 2(b). The patch input admittance for the extended transmission-line model given in Eq. (2a) remain the same with the value of Ψ, given in Eq. (2b) and Eq. (2c), modified as:

$$\Psi = \frac{2G_{VarD}}{\omega G_{VarD}\left(2L_{sh} + L_{VarD}\right) - j} \tag{3}$$

in the forward-biased mode, and

$$\Psi = -\frac{2\omega C_{VarD}}{1 - \omega^2 C_{VarD}\left(2L_{sh} + L_{VarD}\right)} \tag{4}$$

in the reverse-biased mode. All other parameters remain the same as mentioned before.

4.3. Admittance with Two Vias and Multiple Diodes

The microstrip patch antenna has a magnetic symmetry across the centre of the radiating slots [22] and when two thin vias ($D_{\text{Via}} \ll W_P$) are connected near two outer vertices, the extended transmission-line model (considering that two diodes are connected to each via) shown in Figs. 2(a) and 2(b), is further extended and shown in Fig. 2(c). The value of Ψ given in Eq. (2b) and Eq. (2c) can be re-written as:

$$\Psi = \frac{4G_{VarD}}{\omega G_{VarD}\left(2L_{sh} + L_{VarD}\right) - j} \tag{3a}$$

in the forward-biased mode, and

$$\Psi = -\frac{4\omega C_{VarD}}{1 - \omega^2 C_{VarD}\left(2L_{sh} + L_{VarD}\right)} \tag{3b}$$

in the reverse-biased mode. All other parameters remain the same as mentioned before.

5. IMPLEMENTATION AND RESULTS

Primarily, the inset-fed transmission-line model was coded into Matlab using Eqs. (1), (3)–(5). The base antenna designs were manufactured and measurements were compared with the general inset-fed transmission-line model (GETLM) for accuracy. Transmission-line models of the reconfigurable antennas were then further incorporated into Matlab code using Eqs. (2)–(7). Corresponding varactor junction capacitance and forward series resistance values were taken from the Skyworks SMV1232-079LF varactor diode datasheet. 'Base Design I' and 'Base Design II' were manufactured in-house using CNC router isolation milling and chemical etching and the return loss characteristics were measured. Full-wave simulations were conducted using CST Microwave Studio 2015 to compare results obtained with the extended transmission-line model (ETLM). Results obtained for the antennas are discussed in the following subsections. The base resonance frequency (without any modification to the simple patch antenna) for 'Base Design I', 'Antenna I' and 'Antenna III' is 1800 MHz and for 'Base Design II', 'Antenna II', 'Antenna IV' and 'Antenna V' is 2280 MHz. For brevity measured normalized far-field patterns are shown only for 'Antenna I' and the other antennas have similar patterns.

5.1. Base Antenna Designs

The analytically obtained complex impedance (normalized to 50 Ω) for 'Base Design I', obtained through the general inset-fed transmission-line model (GETLM) is compared to the measured impedance (using an Agilent PNA-X vector network analyser) in Fig. 3(a). The transmission-line model results along with the measurement results for the outer vertex shorted patch antenna is shown in Fig. 3(b). Both the results are in good agreement to each other. The fundamental resonance frequency of the antenna is 1723 MHz and the resonance frequency of the vertex shorted antenna is 1797 MHz.

Complex impedance normalized to 50 Ω, for 'Base Design II', obtained through the model along with its measured counterpart is shown in Fig. 3(c). Comparison of the vertex shorted patch antenna results is shown in Fig. 3(d). Similar to the previous one, the agreement is quite good. The fundamental resonance frequency of the antenna is 2320 MHz and the resonance frequency of the vertex shorted antenna is 2410 MHz.

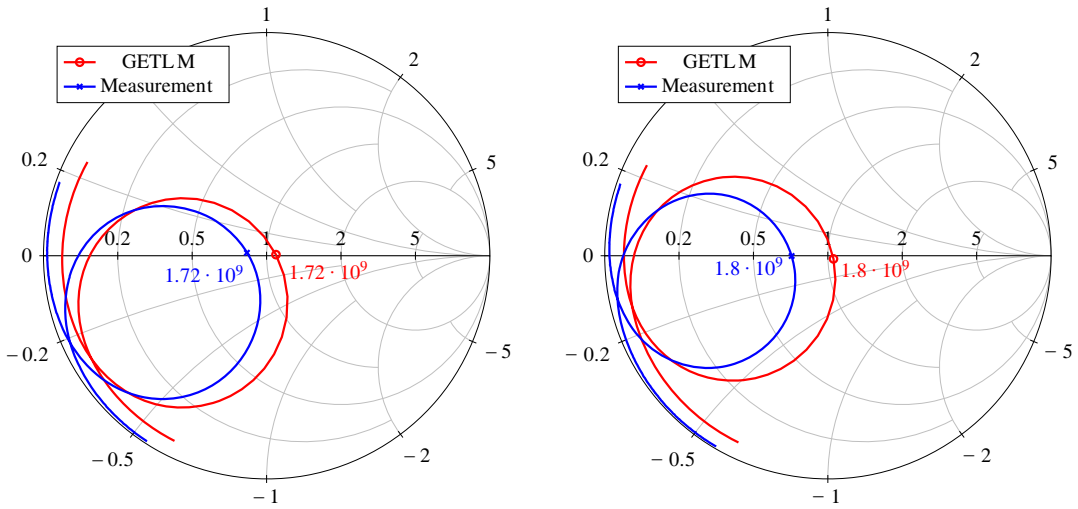

(a) Base Antenna I

(b) Base Antenna I shorted with a thin shorting post at one of the outer vertex

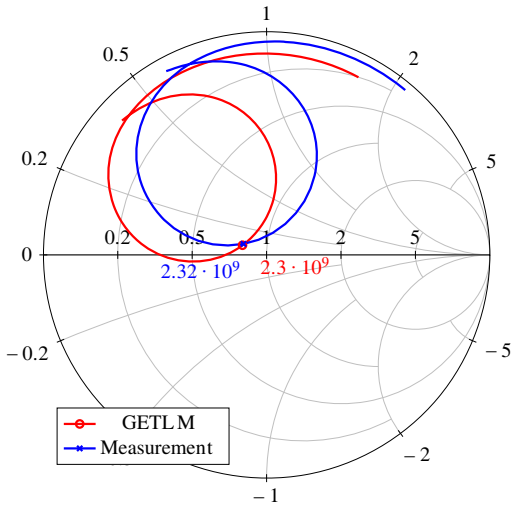

(c) Base Antenna II

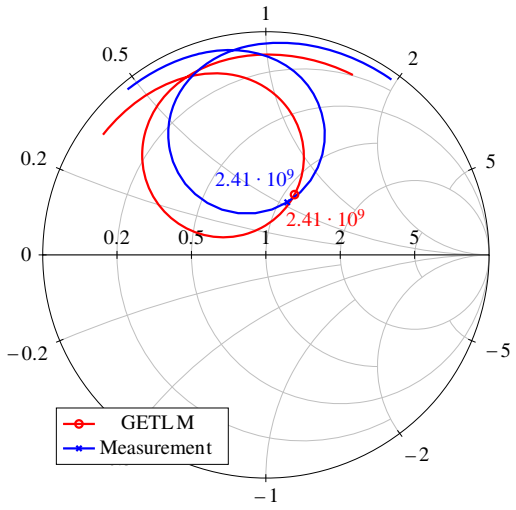

(d) Base Antenna II shorted with a thin shorting post at one of the outer vertex

Figure 3. Complex impedance of Base Design I and II (with and without shorting pin) obtained using the empirical inset-fed transmission-line model and measurements. The Smith Chart is normalized to 50 Ω and shows the complex impedance between 1500 MHz and 2000 MHz for Base Design I, and between 2200 MHz and 2700 MHz for Base Design II, respectively.

These four results verified the accuracy of the inset-feed transmission line model described in Section 3, and it can be extensively used for the reconfigurable antennas. The GETLM is successful for different substrates and resonance frequencies for both conventional and vertex shorted rectangular microstrip antennas.

5.2. Antenna I

Complex impedance for 'Antenna I' is shown in Fig. 4(a) and Fig. 4(b) for the reverse bias voltages of 2 V and 9 V, respectively. The analytically obtained input reflection coefficient magnitude $|S_{11}|$ obtained using the ETLM discussed earlier is shown in Fig. 5(a). Fig. 5(b) shows the measured $|S_{11}|$ obtained from an Agilent PNA-X vector network analyser. The ELTM results are in good agreement with the measured results and a comparison is tabulated in Table 1. Deviations for all the bias conditions is

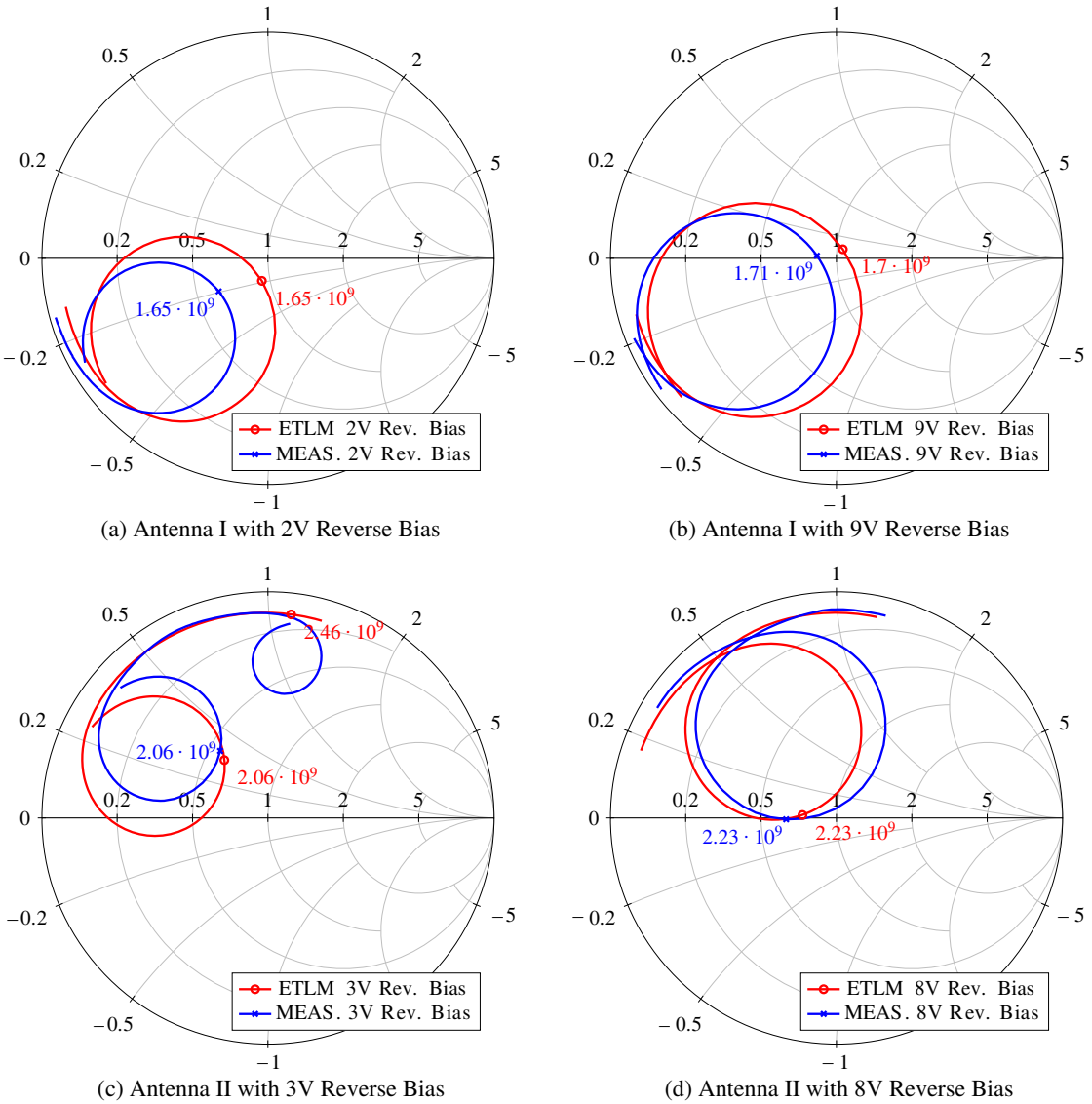

(a) Antenna I with 2V Reverse Bias

(b) Antenna I with 9V Reverse Bias

(c) Antenna II with 3V Reverse Bias

(d) Antenna II with 8V Reverse Bias

Figure 4. Complex impedance of Antenna I & II, under various bias conditions, obtained using ETLM and measurements. The Smith Chart is normalized to 50 Ω and shows the complex impedance between 1600 MHz and 1800 MHz for Antenna I, and between 2000 MHz and 2500 MHz for Antenna II, respectively.

given as a percentage in Table 1. The maximum deviation for the ELTM with respect to simulations is 0.40% and is 0.53% when compared to measurements.

Tuning is achieved between 1650 MHz to 1708 MHz with the varactor diode biased into reversed-mode and reverse voltage swept between 2 V to 9 V. The antenna also resonates at a frequency of 1766 MHz when the varactor diode is forward biased. Fig. 5(d) shows the measured normalized far-field patterns for the reverse-bias voltages of 2 V and 5 V and a forward-bias voltage of 1 V, at the corresponding resonance frequencies of 1650 MHz, 1700 MHz and 1765 MHz, respectively. Peak realized gain is 5.86 dBi, 6.82 dBi and 5.83 dBi at these frequencies, respectively. The pattern is consistent across the entire tuning range but the gain varies slightly due to variation in active device losses.

The variation of realized gain is shown in Fig. 5(c), under different bias conditions. The efficiency of the antenna is low for low reverse-bias voltages but increases with the increase of the tuning voltage. The reason behind this phenomenon is that the intrinsic capacitance of the varactor diode decreases

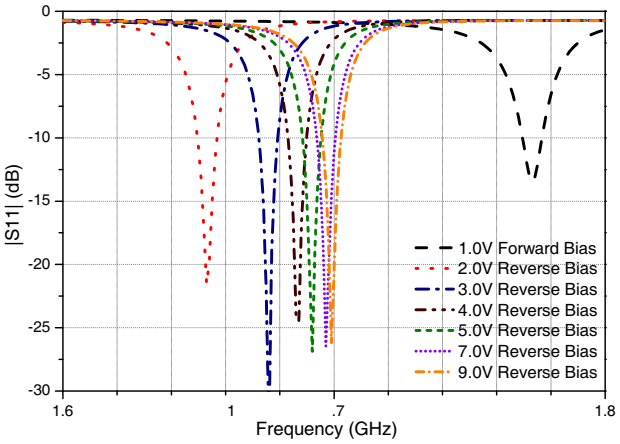

(a) Analytical result obtained using Eq. (2)-(5)

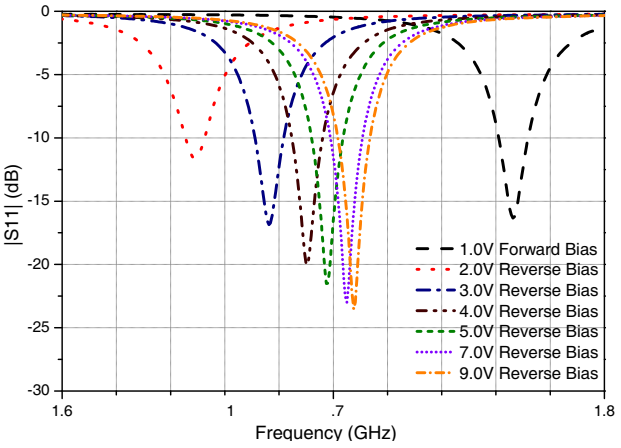

(b) Measured result

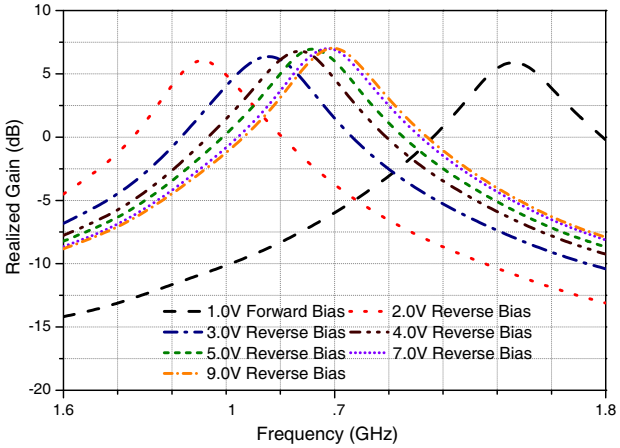

(c) Realized gain over the tunable range obtained using CST MWS 2015

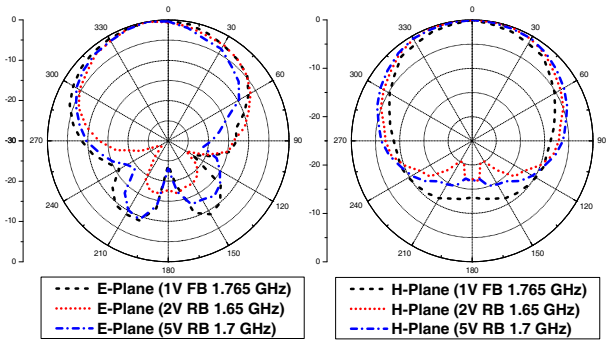

(d) Measured far eld pattern in the E-plane and H-plane

Figure 5. Predicted and measured return loss, realized gain and farfield pattern of 'Antenna I' with a single varactor diode under different bias conditions.

Table 1. Comparison of predicted resonant frequencies for 'Antenna I' along swith those obtained from measurements, under different bias conditions. Percentage deviation of predicted value is relative to simulation and measurement results, respectively.

Bias (V)	Bias Type	ETLM	CST	% Devn.	Measured	% Devn.
1.0	Forward	1773	1766	0.40	1766	0.40
2.0	Reverse	1653	1651	0.12	1650	0.18
3.0	Reverse	1676	1674	0.12	1676	0.00
4.0	Reverse	1687	1686	0.06	1690	0.18
5.0	Reverse	1692	1691	0.06	1698	0.35
7.0	Reverse	1697	1697	0.00	1705	0.47
9.0	Reverse	1699	1699	0.00	1708	0.53

with increasing voltage resulting a very low susceptance and thus it is less prone to allow lossy currents at a given frequency of operation. Additionally, even though the patch is being tuned to operate at a lower frequency, the length of the patch is not ideal to produce maximum radiation and hence the radiation efficiency starts to deteriorate. In forward-biased operation, the loss is due to the forward-bias diode resistance. In the forward bias mode, 'Antenna I' has a total efficiency of 63%. In the 9 V reverse bias, the efficiency is 88% and it is 73% when the reverse bias is 2 V.

5.3. Antenna II

Complex impedance results in the Smith chart are shown in Fig. 4(c) and Fig. 4(d) for the reverse bias voltages of 3 V and 8 V, respectively. Results obtained through ELTM are in good agreement with the measured results and are shown in Fig. 6(a). Fig. 6(b) shows the measured results under different bias conditions. It is interesting to note here that the measured results show few more reverse-bias voltage plots that have a resonance frequency higher than the base frequency of the antenna (2280 MHz), similar to the forward-biased case. This is because of the large junction capacitance of the varactor diode, which behaves more like a bypass capacitor creating an AC short. The ELTM does not perform effectively at this stage and the deviation is more than 3% in some of the test cases. Table 2 compares the ETLM results to simulations and measurements. Two out of nine test cases have a deviation more than 3%.

Figure 6(d) shows the surface current density of the antenna for various configurations. Figs. 6(d), (i) show the surface current of the antenna without any diode bridging the annular gap, even though

Table 2. Comparison of predicted resonant frequencies for 'Antenna II' along with those obtained from measurements, under different bias conditions.

Bias (V)	Bias Type	ETLM	CST	% Devn.	Measured	% Devn.
0.0	Unbiased	2435	2372	2.66	2370	2.74
1.0	Forward	2382	2347	1.49	2350	1.36
1.0	Reverse	2490	2392	4.10	2387	4.32
1.5	Reverse	2531	2403	5.33	2398	5.55
3.0	Reverse	2052	2069	0.82	2060	0.39
4.0	Reverse	2147	2131	0.75	2135	0.56
5.0	Reverse	2187	2164	1.06	2178	0.41
6.0	Reverse	2208	2184	1.10	2203	0.23
8.0	Reverse	2228	2205	1.04	2223	0.22

Table 3. Comparison of predicted resonant frequencies for 'Antenna III' along with those obtained from measurements, under different bias conditions.

Bias (V)	Bias Type	ETLM	CST	% Devn.
0.0	Unbiased	1842	1822	1.10
1.0	Forward	1783	1783	0.00
1.0	Reverse	1905	1861	2.36
2.0	Reverse	1457	1583	7.96
3.0	Reverse	1579	1625	2.83
4.0	Reverse	1630	1649	1.15
5.0	Reverse	1651	1663	0.72
6.0	Reverse	1663	1670	0.42
9.0	Reverse	1677	1681	0.24

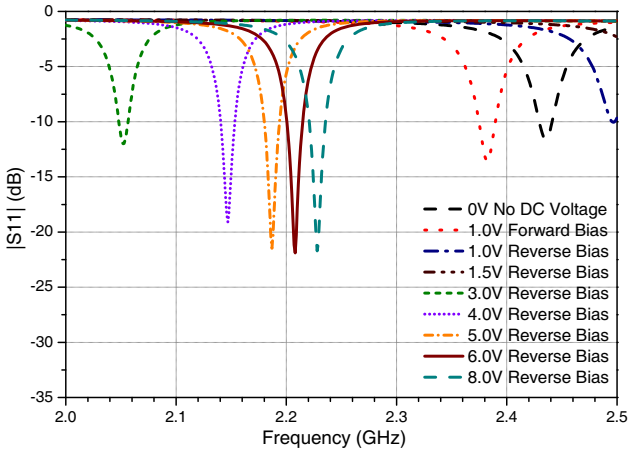

(a) Analytical result obtained using Eq. (2)-(5)

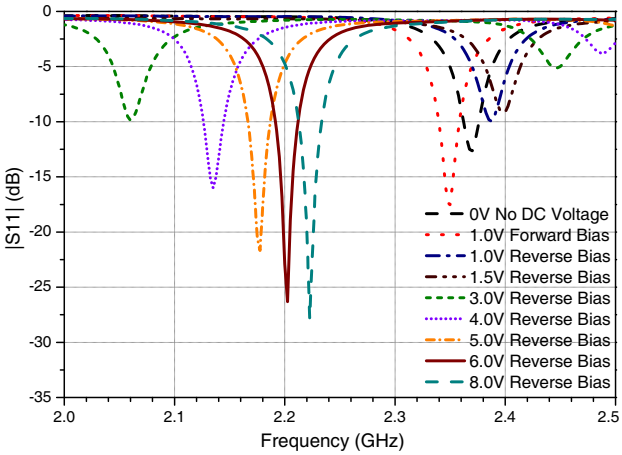

(b) Measured result

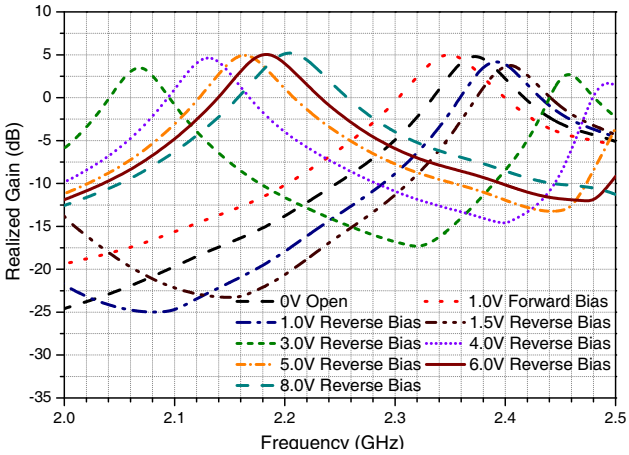

(c) Realized gain over the tunable range obtained using CST MWS 2015

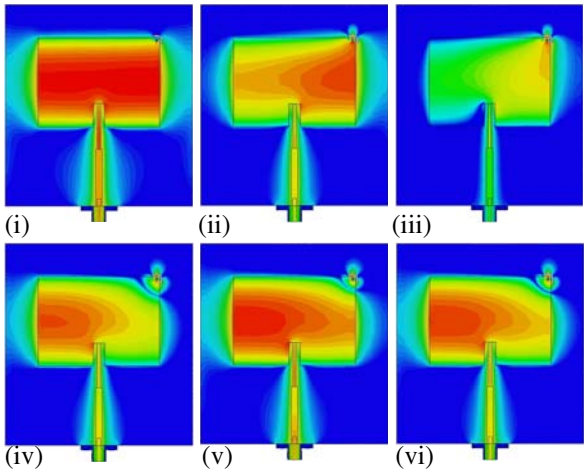

(d) Surface current density with di erent bias conditions

Figure 6. Predicted and measured return loss and realized gain of 'Antenna II' with a single varactor diode under different bias conditions along with the surface current density when the (d), (i) patch antenna resonating at 2280 MHz without any diode connected across the annular gap, (d), (ii) patch antenna resonating at 2205 MHz with the diode reverse biased at 8 V, (d), (iii) patch antenna with the diode reverse biased at 3 V, resonating at 2069 MHz, (d), (iv) patch antenna with the diode unbiased (having a large junction capacitance), resonating at 2372 MHz, (d), (v) patch antenna with the diode forward biased, resonating at 2347 MHz, and (d), (vi) patch antenna with a strip short in place of the diode, resonating at 2345 MHz.

the via is present. In this case, the via does not short to the greater ground plane, and the surface current density is as in a conventional rectangular microstrip patch antenna. The resonance frequency is 2280 MHz. The surface current density with the varactor reverse biased at 8 V is shown in Figs. 6(d), (ii). At this voltage, the resonance frequency is 2205 MHz. The loading of the capacitor at one of the vertex disturbed the uniformity of the current density. Figs. 6(d), (iii) show the current density with a reverse bias of 3 V. This is the lowest voltage and the highest value of junction capacitance (1.51 pF) which can act as a load for this antenna which resonates at 2069 V. Any higher value of the junction capacitance becomes a bypass capacitor. This phenomenon is shown in Figs. 6(d), (iv). With an unbiased varactor, the junction capacitance is 4.15 pF and acts as a bypass capacitor shorting the vertex of the patch

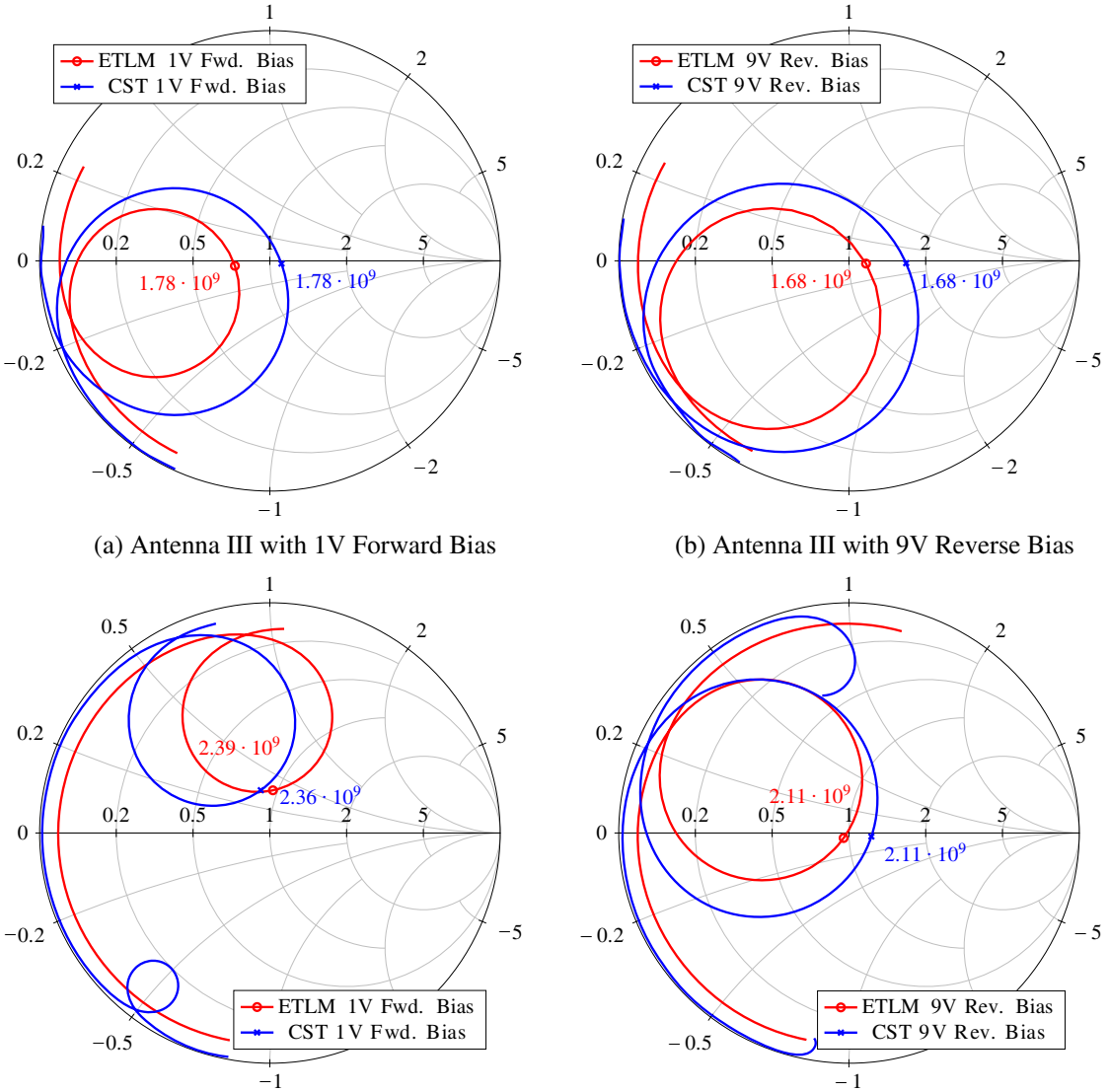

(a) Antenna III with 1V Forward Bias

(b) Antenna III with 9V Reverse Bias

(c) Antenna IV with 1V Forward Bias

(d) Antenna IV with 9V Reverse Bias

Figure 7. Complex impedance of Antenna III & IV, under various bias conditions, obtained using ETLM and measurements. The Smith Chart is normalized to 50 Ω and shows the complex impedance between 1500 MHz and 2000 MHz for Antenna III, and between 1500 MHz and 2500 MHz for Antenna IV, respectively.

antenna, thus reducing the effective radiating area of the patch. In this case the resonance frequency is 2372 MHz. When the varactor diode is forward biased, the surface current distribution is similar to having a bypass capacitor, as shown in Figs. 6(d), (v). The resonance frequency with a forward bias is 2347 MHz. Finally the surface current density with a strip-short (a copper strip soldered in place of the diode as shown in Fig. 1(c)) is shown in Figs. 6(d), (vi). The resonance frequency with a strip-short is 2345 MHz.

This prototype was particularly chosen to demonstrate the bypass effect of the varactor diode and the disability of the transmission-line model in those test cases. This bypassing effect led to tunable resonance frequencies both above and below the base resonance frequency of the patch antenna (i.e., 2280 MHz). This effect cannot be seen in 'Antenna I' as it operates in a lower frequency range. Frequency reconfigurability is achieved between 2060 MHz to 2223 MHz and again from 2370 MHz to 2398 MHz with the varactor diode biased into reversed-mode and reverse voltage swept between 0 V to

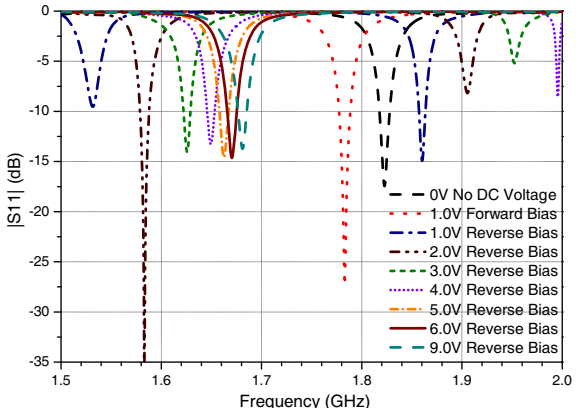

(a) Predicted result for Antenna III using CST MWS & DS 2015

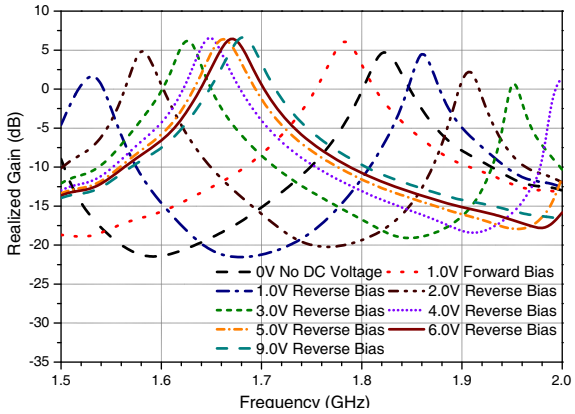

(b) Realized gain for Antenna III over the tunable range obtained using CST MWS 2015

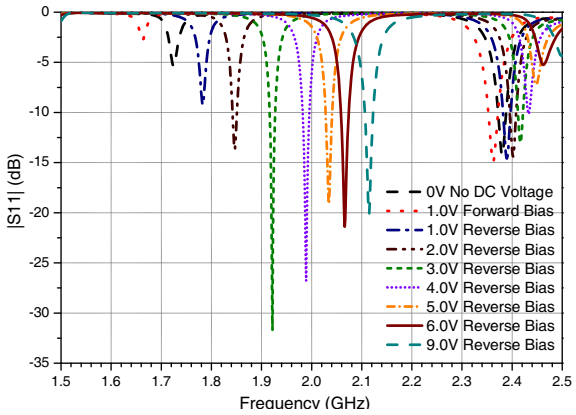

(c) Predicted result for Antenna IV using CST MWS & DS 2015

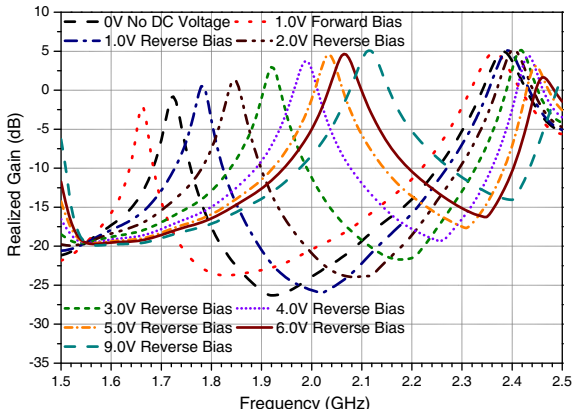

(d) Realized gain for Antenna IV over the tunable range obtained using CST MWS 2015

Figure 8. Predicted return loss and realized gain of 'Antenna III' and 'Antenna IV', under different bias conditions.

8 V, for the manufactured prototype. The antenna also resonates at a frequency of 2350 MHz when the varactor diode is forward biased. The variation of realized gain is shown in Fig. 5(c), under different bias conditions. The forward bias efficiency is 69% and the reverse bias efficiencies are 56% and 74% at 3 V and 8 V, respectively.

5.4. Antenna III

Complex impedance results in the Smith chart are shown in Fig. 7(a) and Fig. 7(b) for the forward bias at 1 V and reverse bias at 9 V, respectively. Table 3 compares the resonance frequencies obtained with the ETLM to the simulation results. In eight out of nine test cases, the transmission-line model has a very good agreement with the simulated complex impedance, with less than 3% deviation with respect to simulations. Four out of nine test cases have less than 1% deviation. Table 3 compares the resonance frequencies obtained with the ETLM to the simulation results. Predicted return loss results are presented in Fig. 8(a) to provide an insight about the tuning range and gain roll-off effects when two varactor diodes are used to connect the via to the greater ground plane. This results in a phenomenon similar to 'Antenna II' where the cumulative capacitance is large enough to create an AC short. The antenna can be tuned between 1530 MHz to 1680 MHz and again from 1823 MHz to 1880 MHz with reverse-bias and to 1780 MHz with forward-bias. The gain roll-off for the antenna across the tuning range is shown in Fig. 8(b). The forward bias efficiency is 67% and the reverse bias efficiencies are 58% and 81% at 2 V and 9 V, respectively.

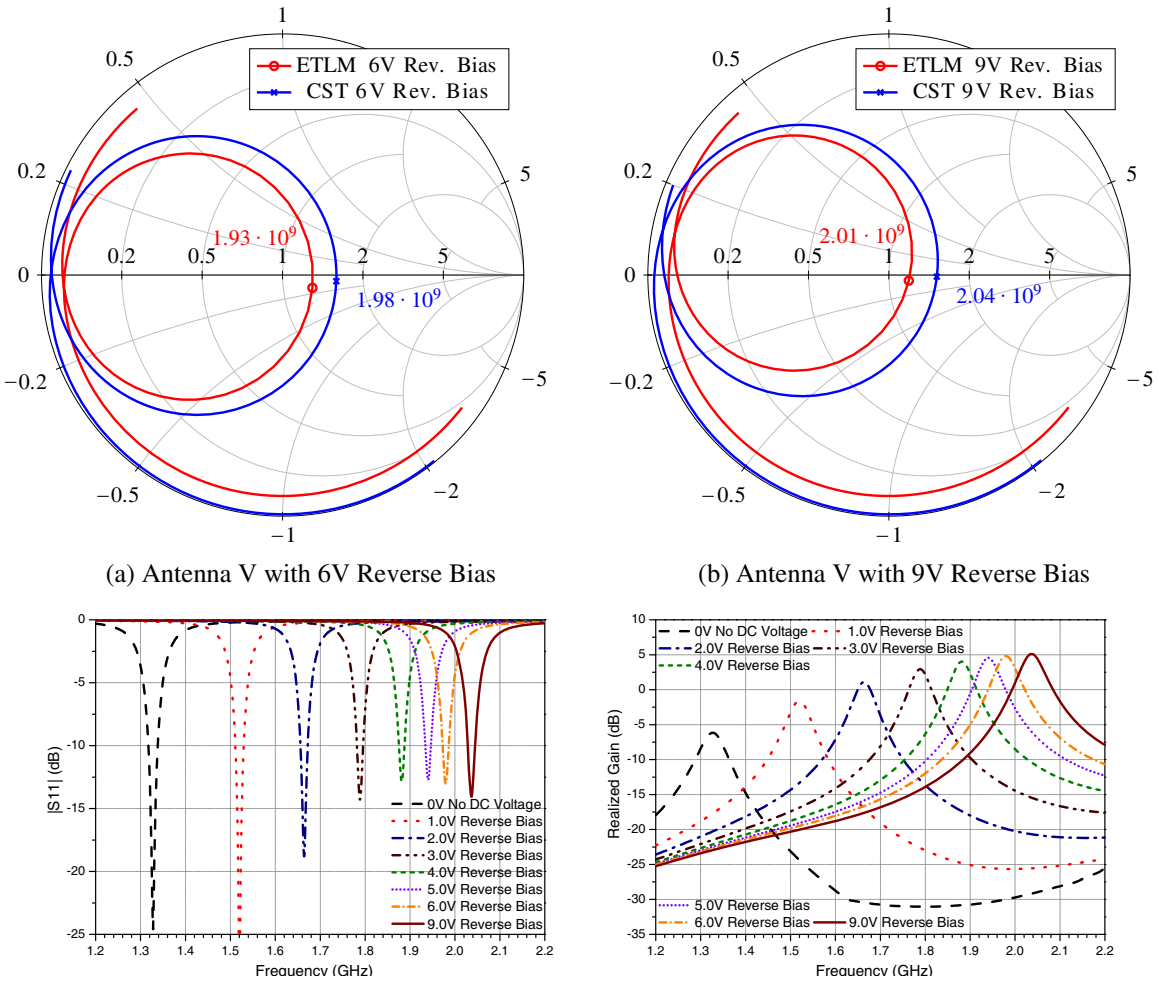

(a) Antenna V with 6V Reverse Bias

(b) Antenna V with 9V Reverse Bias

(c) Predicted result using CST MWS & DS 2015

(d) Realized gain over the tunable range obtained using CST MWS 2015

Figure 9. Complex impedance of Antenna V, predicted return loss and realized gain, under various bias conditions, obtained using ETLM and measurements. The Smith Chart is normalized to 50 Ω and shows the complex impedance between 1200 MHz and 2200 MHz.

Table 4. Comparison of predicted resonant frequencies for 'Antenna IV' along with those obtained from measurements, under different bias conditions.

Bias (V)	Bias Type	ETLM	CST	% Devn.
0.0	Unbiased	2427	2380	1.97
1.0	Forward	2395	2362	1.40
1.0	Reverse	2452	2390	2.59
2.0	Reverse	1406 & 2485	1847 & 2402	23.88 & 3.46
3.0	Reverse	1598 & 2521	1922 & 2417	16.86 & 4.30
4.0	Reverse	1804 & 2585	1989 & 2433	9.30 & 6.25
5.0	Reverse	1986	2034	2.36
6.0	Reverse	2042	2066	1.16
9.0	Reverse	2111	2114	0.14

5.5. Antenna IV

Complex impedance results are shown in Fig. 7(c) and Fig. 7(d) for 1 V forward bias and 9 V reverse bias, respectively. Table 4 shows the comparison between ETLM and simulations for multiple test cases. Only five out of nine test cases have deviations less than 3%. Only one test case has a deviation less than 1%. But the complex impedance for ETLM with less that 3% deviation are in good agreement to simulations, when plotted on a Smith chart. This antenna can be tuned between 1800 MHz to 2115 MHz and again from 2380 MHz to 2418 MHz with reverse-bias and to 2362 MHz with forward-bias. Fig. 8(c) shows the return loss predicted by CST Microwave Studio and Design Studio 2015, under different bias conditions. The gain roll-off for the antenna across the tuning range is shown in Fig. 8(d). The forward bias efficiency is 65% and the reverse bias efficiencies are 33% and 73% at 2 V and 9 V, respectively.

5.6. Antenna V

Table 5 compares the ETLM results with CST simulations. None of the test cases have a deviation less than 1%. Only two of the test cases have deviations less than 3% when compared to simulations, but their complex impedance are in fair agreement to simulations when plotted on a Smith chart. Fig. 9(a) and Fig. 9(b) show the comparison for reverse-bias at 6 V and 9 V, respectively. Fig. 9(c) shows the tunable range for the antenna under various reverse-bias conditions, as obtained from simulations. The antenna can be tuned between 1328 MHz (with no bias) voltage to 2037 MHz (with 9 V reverse-bias). The gain roll-off shown in Fig. 9(d) is quite significant. The realized peak gain varies between −6 dBi at (0 V bias) to 5.1 dBi (with 9 V reverse-bias), respectively. The reverse bias efficiencies are 8% and 74% at 0 V and 9 V, respectively.

Table 5. Comparison of predicted resonant frequencies for 'Antenna IV' along with those obtained from measurements, under different bias conditions.

Bias (V)	Bias Type	ETLM	CST	% Devn.
0.0	Unbiased	927	1328	30.20
1.0	Reverse	1225	1520	19.41
2.0	Reverse	1442	1664	13.34
3.0	Reverse	1640	1789	8.33
4.0	Reverse	1785	1881	5.10
5.0	Reverse	1872	1940	3.51
6.0	Reverse	1928	1979	2.58
9.0	Reverse	2006	2037	1.52

6. CONCLUSION

A few extended transmission-line models are presented for inset-fed rectangular microstrip patch antennas loaded with one or more varactor diodes. More than one type of substrate and layouts were used to validate the models rigorously. The transmission-line models agrees with the $\cos^4$ impedance variation for inset-fed microstrip antennas with an addition of a corrective feed length to the inner radiating edge. Verification of the model was concluded with its complex reflection coefficient in good agreements to the measured results. Further extension of the transmission-line models with varactors were concluded with 69% of forty two (42) test cases having less than 3% deviation from measured or simulated results. Further studies are ongoing to find an explanation about the rest of 31% test cases where the transmission-line models were not as successful. Quick design solutions are possible with the extended transmission-line model to achieve reasonable accuracy without using the time-consuming full wave solvers.

ACKNOWLEDGMENT

This research was supported by the Australian Research Council and International Macquarie Research Excellence Scholarship.

REFERENCES

1. Munson, R., "Conformal microstrip antennas and microstrip phased arrays," *IEEE Trans. Antennas Propag.*, Vol. 22, No. 1, 74–78, 1974.
2. Derneryd, A. G., "Linearly polarized microstrip antennas," *IEEE Trans. Antennas Propag.*, Vol. 24, No. 6, 846–851, 1976.
3. Derneryd, A. G., "A theoretical investigation of the rectangular microstrip antenna element," *IEEE Trans. Antennas Propag.*, Vol. 26, No. 4, 532–535, 1978.
4. Carver K. R. and J. Mink, "Microstrip antenna technology," *IEEE Trans. Antennas Propag.*, Vol. 29, No. 1, 2–24, 1981.
5. Balanis, C. A., *Antenna Theory: Analysis and Design*, Wiley-Interscience, 2005.
6. Ghatak, R. and M. Pal, "Revisiting relations for modeling the input resistance of a rectangular microstrip antenna [Antenna Designer's Notebook]," *IEEE Antennas Propag. Mag.*, Vol. 57, No. 4, 116–119, 2015.
7. Ying, H., D. R. Jackson, J. T. Williams, S. A. Long, and V. R. Komanduri, "Characterization of the input impedance of the inset-fed rectangular microstrip antenna," *IEEE Trans. Antennas Propag.*, Vol. 56, No. 10, 3314–3318, 2008.
8. Basilio, L. I., M. A. Khayat, J. T. Williams, and S. A. Long, "The dependence of the input impedance on feed position of probe and microstrip line-fed patch antennas," *IEEE Trans. Antennas Propag.*, Vol. 49, No. 1, 45–47, 2001.
9. Garvin, C., R. Munson, L. Ostwald, and K. Schroeder, "Missile base mounted microstrip antennas," *IEEE Trans. Antennas Propag.*, Vol. 25, No. 5, 604–610, 1977.
10. Kan, H. K. and R. B. Waterhouse, "Size reduction technique for shorted patches," *Electron. Lett.*, Vol. 35, No. 12, 948–949, 1999.
11. Reed, S., L. Desclos, C. Terret, and S. Toutain, "Patch antenna size reduction by means of inductive slots," *Microw. Opt. Technol. Lett.*, Vol. 29, No. 2, 79–81, 2001.
12. Desclos, L., Y. Mahe, S. Reed, G. Poilasne, and S. Toutain, "Patch antenna size reduction by combining inductive loading and short-points technique," *Microw. Opt. Technol. Lett.*, Vol. 30, No. 6, 385–386, 2001.
13. Schaubert, D., F. Farrar, A. Sindoris, and S. Hayes, "Microstrip antennas with frequency agility and polarization diversity," *IEEE Trans. Antennas Propag.*, Vol. 29, No. 1, 118–123, 1981.
14. Sengupta, D. L., "Resonant frequency of a tunable rectangular patch antenna," *Electron. Lett.*, Vol. 20, No. 15, 614–615, 1984.
15. Lan, G. L. and D. L. Sengupta, "Tunable circular patch antennas," *Electron. Lett.*, Vol. 21, No. 22, 1022–1023, 1985.
16. Garg, R., et al., *Microstrip Antenna Design Handbook*, Artech House Inc., 2001.
17. Chakravarty, T. and A. De, "Design of tunable modes and dual-band circular patch antenna using shorting posts," *IEE P. — Microw. Anten. P.*, Vol. 146, No. 3, 224–228, 1999.
18. Chakravarty, T. and A. De, "Resonant frequency of a shorted circular patch with the use of a modified impedance expression for a metallic post," *Microw. Opt. Technol. Lett.*, Vol. 33, No. 4, 252–256, 2002.
19. Ghosh, D., et al., "Physical and quantitative analysis of compact rectangular microstrip antenna with shorted non-radiating edges for reduced cross-polarized radiation using modified cavity model," *IEEE Antennas and Propagation Magazine*, Vol. 56, No. 4, 61–72, 2014.

20. Wang, Y. J. and C. K. Lee, "Compact and broadband microstrip patch antenna for the 3G IMT-2000 handsets applying styrofoam and shorting-posts," *Progress In Electromagnetics Research*, Vol. 47, 75–85, 2004.
21. Majumdar, B. and K. P. Esselle, "A dual-mode reconfigurable patch antenna and an extended transmission line model," *Microw. Opt. Technol. Lett.*, Vol. 58, No. 1, 57–61, 2016.
22. Majumdar, B. and K. P. Esselle, "Modelling the effect of a thin shorting post in an arbitrary position along the outer radiating edge of a rectangular patch antenna," *Proc. Intnl. Symp. Antennas Propag. No. ISAP 2015)*, 84–86, Hobart, Australia, Nov. 2015.
23. Chen, W.-F., D. Yu, and S.-X. Gong, "An omnidirectional triple-band circular patch antenna based on open elliptical-ring slots and the shorting vias," *Progress In Electromagnetics Research*, Vol. 150, 197–203, 2015.
24. Biswas, M. and A. Mandal, "Experimental and theoretical investigation to predict the effect of superstrate on the impedance, bandwidth, and gain characteristics for a rectangular patch antenna," *Journal of Electromagnetic Waves and Applications*, Vol. 29, No. 16, 2093–2109, 2015.
25. Richards, W., L. Yuen, and D. Harrison, "An improved theory for microstrip antennas and applications," *IEEE Trans. Antennas Propag.*, Vol. 29, No. 1, 38–46, 1981.
26. Haskins, P. M., P. S. Hall, and J. S. Dahele, "Polarisation-agile active patch antenna," *Electron. Lett.*, Vol. 30, No. 2, 98–99, 1994.
27. Haskins, P. M. and J. S. Dahele, "Varactor-diode loaded passive polarisation-agile patch antenna," *Electron. Lett.*, Vol. 30, No. 13, 1074–1075, 1994.
28. Haskins, P. M. and J. S. Dahele, "Four-element varactor diode loaded polarisation-agile microstrip antenna array," *Electron. Lett.*, Vol. 33, No. 14, 1186–1187, 1997.
29. Haskins, P. M., P. S. Hall, and J. S. Dahele, "Active patch antenna element with diode tuning," *Electron. Lett.*, Vol. 27, No. 20, 1846–1848, 1991.
30. Waterhouse, R. B., "Modelling of Schottky-Barrier diode loaded microstrip array elements," *Electron. Lett.*, Vol. 28, No. 19, 1799–1801, 1992.
31. Waterhouse, R. B. and N. V. Shuley, "Dual frequency microstrip rectangular patches," *Electron. Lett.*, Vol. 28, No. 7, 606–607, 1992.
32. Waterhouse, R. B. and N. V. Shuley, "Scan performance of infinite arrays of microstrip patch elements loaded with varactor diodes," *IEEE Trans. Antennas Propag.*, Vol. 41, No. 9, 1273–1280, 1993.
33. Waterhouse, R. B. and N. V. Shuley, "Full characterisation of varactor-loaded, probe-fed, rectangular, microstrip patch antennas," *IEE P. — Microw. Anten. P.*, Vol. 141, No. 5, 367–373, 1994.
34. Chakravarty, T., S. K. Sanyal, and A. De, "Resonant modes of circular microstrip radiator loaded with varactor diode," *Radio Sci.*, Vol. 42, No. 4, RS4024, 2007.
35. Waterhouse, R. B., "The use of shorting posts to improve the scanning range of probe-fed microstrip patch phased arrays," *IEEE Trans. Antennas Propag.*, Vol. 44, No. 3, 302–309, 1996.
36. Wei, W.-B., Q.-Z. Liu, Y.-Z. Yin, and H.-J. Zhou, "Reconfigurable microstrip patch antenna with switchable polarization," *Progress In Electromagnetics Research*, Vol. 75, 63–68, 2007.
37. Wang, K.-L. and Y.-F. Lin, "Small broadband rectangular microstrip antenna with chip-resistor loading," *Electron. Lett.*, Vol. 33, No. 19, 1593–1594, 1997.
38. Hum, S. V., J. Z. Chu, R. H. Johnston, and M. Okoniewski, "Efficiency of a resistively loaded microstrip patch antenna," *IEEE Antennas Wireless Propag. Lett.*, Vol. 2, No. 1, 22–25, 2003.